

# Heuristic Representation of the Swirl Velocity in the Core of the Bidirectional Vortex

Brian A. Maicke\* and Joseph Majdalani†  
 University of Tennessee Space Institute, Tullahoma, TN 37388

In this article, we discuss the merits of a heuristic, piecewise representation of the swirl velocity in the core of the bidirectional vortex. This combined vortex representation is based on the notion that a uniform, Couette-like, shear stress distribution may be assumed in the inner vortex region, especially at high Reynolds numbers. At the outset, direct integration of the shear stress enables us to retrieve an expression for the swirl velocity that overcomes the inviscid singularity at the centerline. The solution we obtain must be patched to the outer, free vortex approximation at some intermediate position in the chamber. The resulting piecewise distribution is then used to represent the swirl velocity throughout the chamber. Two Rankine-type patching schemes are explored for this heuristic model. In the first, the core solution, along with its first derivative, are patched to the free vortex at the mantle location of 0.707 found by Vyas and Majdalani (Vyas, A. B., and Majdalani, J., "Exact Solution of the Bidirectional Vortex," *AIAA Journal*, Vol. 44, No. 10, 2006, pp. 2208-2216). In the second, the patching is performed at a point that is representative of the thickness of the forced vortex core. The more general representation provides the freedom of using either laminar or turbulent models to estimate the thickness of the core boundary layer at a given vortex Reynolds number. The first model that we explore assumes that the outer, annular region of the bidirectional vortex is driven by free vortex motion, whereas the inner region (inside the mantle) is entirely dominated by constant shear. Being purely inviscid and insensitive to the vortex Reynolds number, it is discarded in favor of a more portable model that can be set to mimic laminar or turbulent profiles. The second, more general approximation is subsequently compared to the existing laminar solution derived directly from first principles. Its pressure distribution is calculated and shown to be non-singular even in the purely inviscid case. The versatility of the piecewise solution is illustrated by specifying a constant shear radius that scales with the existing laminar core layer thickness. Other heuristic schemes are discussed and the conclusion is reached that further refinements for high Reynolds number flows must await the advent of sufficient laboratory and numerical experiments.

## Nomenclature

$a$	= chamber radius
$A_i$	= inlet area
$b$	= chamber outlet radius
$l$	= chamber aspect ratio, $L/a$
$L$	= chamber length
$p$	= normalized pressure, $\bar{p}/(\rho U^2)$
$\bar{Q}_i$	= inlet volumetric flow rate
$Q_i$	= normalized volumetric flow rate in, $\bar{Q}_i/(Ua^2) = \sigma^{-1}$
$Q_o$	= normalized volumetric flow rate out, $\bar{Q}_o/(Ua^2)$

\*Doctoral Research Assistant, Department of Mechanical, Aerospace and Biomedical Engineering. Member AIAA.

†Jack D. Whitfield Professor of High Speed Flows, Department of Mechanical, Aerospace and Biomedical Engineering. Member AIAA. Fellow ASME.

$Re$  = injection Reynolds number,  $Ua/\nu = 1/\varepsilon$   
 $r, z$  = normalized radial or axial coordinates,  $\bar{r}/a, \bar{z}/a$   
 $S$  = swirl number,  $\pi ab/A_i = \pi\beta\sigma$   
 $\mathbf{u}$  = normalized velocity  $(\bar{u}_r, \bar{u}_z, \bar{u}_\theta)/U$   
 $u_\theta$  = normalized swirl/spin/tangential velocity,  $\bar{u}_\theta/U$   
 $U$  = mean inflow velocity,  $\bar{u}_\theta(a, L)$   
 $V$  = vortex Reynolds number,  $Q_i Re(a/L) = (\varepsilon\sigma l)^{-1}$

#### Greek

$\beta$  = normalized outlet radius,  $b/a$   
 $\delta_c$  = normalized core radius,  $\bar{\delta}_c/a$   
 $\varepsilon$  = perturbation parameter,  $1/Re = \nu/(Ua)$   
 $\kappa$  = inflow parameter,  $Q_i/(2\pi l) = (2\pi\sigma l)^{-1}$   
 $\nu$  = kinematic viscosity,  $\mu/\rho$   
 $\rho$  = density  
 $\sigma$  = modified swirl number,  $Q_i^{-1} = S/(\pi\beta)$

#### Subscripts and Symbols

$i$  = inlet property  
 $r$  = radial component or partial derivative  
 $z$  = axial component or partial derivative  
 $\theta$  = azimuthal component or partial derivative  
 $-$  = overbars denote dimensional variables

#### Superscripts

$c$  = composite  
 $i$  = inner core  
 $w$  = near sidewall

## I. Introduction

FROM the pioneering days of Rankine<sup>1</sup> to the present era, swirling flows have remained the subject of ceaseless scientific inquiry both because of their interesting theoretical challenges and their effective utilization in several industrial applications. Historically, the earliest theoretical models have been fundamentally connected with unbounded geophysical flows that spontaneously occur in nature. In this vein, hurricanes and tornadoes have been sporadically modeled using a variety of vortex flowfields.<sup>2</sup> Even stellar phenomena have been subjected to similar exploratory lines of inquiry.<sup>3</sup> While large-scale vortex patterns have constituted the motivation for much of the earlier work, modern investigations have constantly strived to harness the power of swirl in emerging products and mechanical equipment, both domestic and commercial. One may also classify applications into those that employ unidirectional swirl (e.g., swirl combustors) and those that rely on a more complex, self-reversing motion often termed bidirectional.

In the context of wall-bounded bidirectional swirl, one may cite the work of ter Linden<sup>4</sup> that has focused on studying the efficiency of cyclone separators. Later, Bloor and Ingham<sup>5</sup> have analyzed the incompressible fluid motion in conical cyclones using spherical coordinates. More recently, Vyas and Majdalani,<sup>6,7</sup> Vyas, Majdalani and Chiaverini,<sup>8</sup> Majdalani and Rienstra,<sup>9</sup> and Batterson and Majdalani<sup>10</sup> have developed both exact and asymptotic solutions to describe bidirectional flow motions in cylindrical and spherical geometries. Their work has been motivated by a propulsive application, specifically by the need to extend the understanding of gaseous motions in the Vortex Combustion Cold-Wall Chamber (VCCWC). This innovative liquid thrust engine is being developed by Chiaverini *et al.*<sup>11</sup> under the auspices of Orbital Technologies Corporation.

While witnessing a continually renewed interest in cyclonic flows, especially of the confined type, there can also be seen a dearth of rigorous analytical models to describe these flowfields. One reason for this impropriety may be

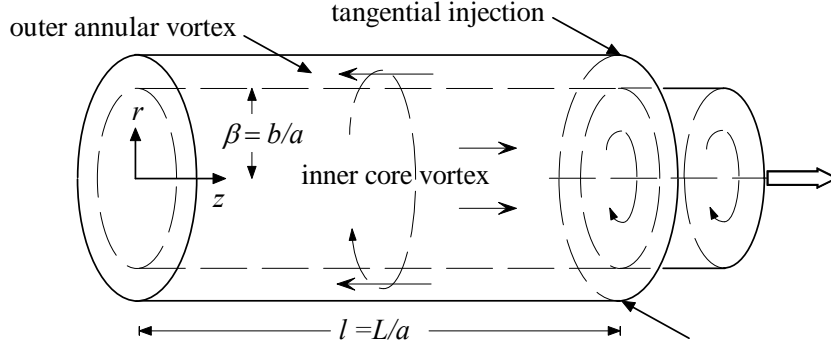


Figure 1. Geometric characteristics of the bidirectional vortex chamber.

attributed to the complexity in the required and the complacency in the available. Given that seemingly inviscid solutions regularly capture basic features of swirl, more elaborate models are often deemed either intractable or unnecessary. In practice, inviscid solutions may be sufficiently suitable for unbounded, swirling flows, but they can fail to capture the physics of confined motions. Because the flowfield is tightly surrounded by solid boundaries, the effects of no slip at the walls and singularities at the core can significantly alter the bulk motion. The characteristics of the core are relatively well understood and have been described by Vatisas *et al.*,<sup>12</sup> Ogawa,<sup>13</sup> Hoekstra *et al.*,<sup>14</sup> and more recently by Derksen and Van den Akker,<sup>15</sup> Fang *et al.*,<sup>16</sup> Rom *et al.*,<sup>17</sup> Murray *et al.*,<sup>18</sup> and Hu *et al.*<sup>19</sup> Nonetheless, a rigorous analytical model for the core is still lacking, especially under high speed conditions. Another reason that new models for confined vortex flows are scant may be linked to the complexity of their governing equations. Despite this complication, Vyas and Majdalani<sup>6,7</sup> have managed to develop an exact inviscid model, followed by a laminar boundary layer model to capture the effects of viscosity on the tangential velocity in the bidirectional vortex chamber. Along similar lines, Batterson and Majdalani<sup>10</sup> have extended the viscous analysis to account for axial and radial boundary layers. These solutions have not only furthered our understanding of the flowfield but they have also opened up new lines of inquiry.

Since the existing solutions stem from fundamental equations that govern laminar flow motion, it would be useful to follow tradition and employ them as a springboard for developing approximations to turbulent flows. With this in mind, it is the goal of this study to present an alternate model that can possibly mimic the inner vortex behavior in a bidirectional vortex chamber. The model will be based on the notion that a constant shear stress may be assumed in the inner vortex region. A Rankine-type patching radius will then be specified to grant the model generality in reproducing the essential features of a swirl-dominated pattern. Two specific examples of the patching technique will be described. In the first, the piecewise approximation is compared to the viscous core boundary layer treatment of Vyas, Majdalani and Chiaverini.<sup>8</sup> In the second, the heuristic model is set to predict turbulent-like behavior. Other matching schemes may be conceived, but these are deferred to later work. In the interim, it may be helpful to pursue further refinements at the outset of extensive experimental tests to validate and anchor the model for high vortex Reynolds number flows.

## II. Mathematical Model

### A. Geometry

This work focuses on the axisymmetric, incompressible, steady, rotational flow spiraling inside a cylindrical chamber of length  $L$  and radius  $a$ . The origin of the coordinate system is fixed at the center of the inert headwall, and a partially open downstream end is taken to have a radius  $b$ . The radial and axial directions are denoted by  $\bar{r}$  and  $\bar{z}$  respectively. A single phase, non-chemically reactive fluid is injected at the base of the chamber, at  $\bar{r} = a$ , in a purely tangential manner and at an average circumferential velocity of  $\bar{u}_\theta = U$ . The attendant geometric parameters consist of the fraction of the radius open at the base, defined as  $\beta = b/a$ , and the aspect ratio of the chamber, given by  $l = L/a$ . Both are shown in Fig. 1.

### B. Basic Formulation

The normalization follows precisely that presented by Vyas and Majdalani.<sup>6</sup> For the reader's convenience, the dimensional governing equations are reproduced here, assuming axisymmetric conditions and an axially invariant swirl velocity:

$$\bar{u}_r \frac{\partial \bar{u}_r}{\partial \bar{r}} + \bar{u}_z \frac{\partial \bar{u}_r}{\partial \bar{z}} - \frac{\bar{u}_\theta^2}{\bar{r}} = -\frac{1}{\rho} \frac{\partial \bar{p}}{\partial \bar{r}} \quad (1)$$

$$\bar{u}_r \left( \frac{\partial \bar{u}_\theta}{\partial \bar{r}} + \frac{\bar{u}_\theta}{\bar{r}} \right) = 0 \quad (2)$$

$$\bar{u}_r \frac{\partial \bar{u}_z}{\partial \bar{r}} + \bar{u}_z \frac{\partial \bar{u}_z}{\partial \bar{z}} = -\frac{1}{\rho} \frac{\partial \bar{p}}{\partial \bar{z}} \quad (3)$$

When normalized, these become

$$u_r \frac{\partial u_r}{\partial r} + u_z \frac{\partial u_r}{\partial z} - \frac{u_\theta^2}{r} = -\frac{\partial p}{\partial r} \quad (4)$$

$$u_r \left( \frac{\partial u_\theta}{\partial r} + \frac{u_\theta}{r} \right) = 0 \quad (5)$$

$$u_r \frac{\partial u_z}{\partial r} + u_z \frac{\partial u_z}{\partial z} = -\frac{\partial p}{\partial z} \quad (6)$$

where

$$z = \frac{\bar{z}}{a}; \quad r = \frac{\bar{r}}{a}; \quad \nabla = a \bar{\nabla}; \quad \beta = \frac{b}{a}; \quad u_r = \frac{\bar{u}_r}{U}; \quad u_\theta = \frac{\bar{u}_\theta}{U}; \quad u_z = \frac{\bar{u}_z}{U}; \quad p = \frac{\bar{p}}{\rho U^2}; \quad Q_i = \frac{\bar{Q}_i}{U a^2} = \frac{A_i}{a^2}; \quad Q_o = \frac{\bar{Q}_o}{U a^2} \quad (7)$$

$$u_r = -\frac{1}{r} \frac{\partial \psi}{\partial z}; \quad u_z = \frac{1}{r} \frac{\partial \psi}{\partial r} \quad (8)$$

and so

$$\frac{\partial^2 \psi}{\partial z^2} + \frac{\partial^2 \psi}{\partial r^2} - \frac{1}{r} \frac{\partial \psi}{\partial r} + C^2 r^2 \psi = 0 \quad (9)$$

As usual, the swirl velocity is assumed to be independent of both axial and azimuthal variations. As a result, Eq. (2) is decoupled from the other velocity terms. This enables us to employ the stream function-vorticity relation, given by Eq. (9), to solve for the axial and radial components. It is this  $(r, z)$  versus  $\theta$  separation that permits advancing a swirl velocity model after Vyas and Majdalani.<sup>6</sup> The exact inviscid solution is simply

$$\left\{ \begin{aligned} \mathbf{u} &= -\kappa \frac{\sin(\pi r^2)}{r} \mathbf{e}_r + \frac{1}{r} \mathbf{e}_\theta + 2\pi \kappa z \cos(\pi r^2) \mathbf{e}_z \\ \Delta p &= -\frac{1}{2r^2} \left\{ 1 + \frac{1}{2} \kappa^2 \left[ 8\pi^2 r^2 z^2 + 1 - \cos(2\pi r^2) \right] \right\} \end{aligned} \right. \quad (10)$$

The corresponding quasi-viscous solution that captures the forced vortex near the core has also been derived by Vyas, Majdalani and Chiaverini.<sup>8</sup> It can be written as

$$\left\{ \begin{aligned} \mathbf{u} &= -\kappa \frac{\sin(\pi r^2)}{r} \mathbf{e}_r + \frac{1}{r} \left( 1 - e^{-\frac{1}{4} V r^2} \right) \mathbf{e}_\theta + 2\pi \kappa z \cos(\pi r^2) \mathbf{e}_z \\ \Delta p &= -\frac{1}{2r^2} \left\{ \begin{aligned} &1 + \frac{1}{2} \kappa^2 \left[ 8\pi^2 r^2 z^2 + 1 - \cos(2\pi r^2) \right] \\ &+ e^{-\frac{1}{2} V r^2} - 2e^{-\frac{1}{4} V r^2} + \frac{1}{2} r^2 V \left[ \text{Ei}\left(-\frac{1}{2} V r^2\right) - \text{Ei}\left(-\frac{1}{4} V r^2\right) \right] \end{aligned} \right\} \end{aligned} \right. \quad (11)$$

where the vortex Reynolds number is given by

$$V = \frac{Re}{\sigma} \frac{a}{L} = \frac{\bar{Q}_i}{Lv} \quad (12)$$

In what follows, Eq. (11) will be referred to as the laminar core model (LCM).

### III. Constant Shear Stress Model

The free vortex motion in the outer domain is dictated by the inviscid solution which is summarized in the previous section. Our main focus here is directed to the inner region, specifically to the development of a model that can capture the behavior of the flow in the core vortex at high Reynolds numbers. We also require the model to remain consistent with the outer motion, merging smoothly with the outer vortex without becoming unbounded at

the centerline. Since the flow under turbulent conditions can deviate from the inviscid representation, one must carefully conceive a suitable model. Following Townsend<sup>20</sup> or Tennekes and Lumley,<sup>21</sup> one may examine

$$(\mathbf{u} \cdot \nabla) \mathbf{u} = -\nabla p + \nabla \cdot \boldsymbol{\tau} \quad (13)$$

For fully developed motion in the tangential direction, it follows that an equilibrium may be maintained between shear and pressure terms under either laminar or turbulent conditions. Then considering a flow with a zero tangential pressure gradient, the dominant shear stress in the tangential direction may be assumed to be spatially uniform. This enables us to set

$$\tau_{r\theta} = \varepsilon \left[ \frac{1}{r} \frac{\partial u_r}{\partial \theta} + r \frac{\partial}{\partial r} \left( \frac{u_\theta}{r} \right) \right] = \varepsilon r \frac{\partial}{\partial r} \left( \frac{u_\theta}{r} \right) = C_1 \quad (14)$$

where the viscous parameter  $\varepsilon$  is small, being inversely proportional to the Reynolds number

$$\varepsilon = \frac{1}{Re} = \frac{\nu}{Ua} \quad (15)$$

It may be instructive to note that the forced vortex solution, for which vorticity is uniformly distributed in the core region,  $u_\theta \propto r$ , may be restored from Eq. (14) by setting  $C_1 = 0$ . To obtain a more general expression, we assume Couette-like shear in the core region.<sup>20-22</sup> We then integrate Eq. (14) to obtain

$$u_\theta^{(i)} = r \left[ \frac{C_1}{\varepsilon} \ln(r) + C_2 \right] \quad (16)$$

Here, the superscript  $(i)$  denotes a solution in the inner region. The two undetermined constants can be manipulated to patch the inner solution with the outer, free vortex expression at their intersection point. Since the patch-point radius is not known a priori, it must be carefully specified. The most elementary choice will be to patch the two solutions at the theoretical mantle location,  $r = \beta$ , where the flow changes direction. Consequently, the core flow will coincide with the inner vortex bounded by the mantle and the free vortex will be strictly confined to the annular region situated between the mantle and the sidewall. To facilitate this patching, we equate both the velocities and the slopes of the inner  $(i)$  and outer  $(o)$  solutions at  $r = \beta$ . These conditions translate into

$$\begin{cases} u_\theta^{(i)}(\beta) = u_\theta^{(o)}(\beta) \\ u_\theta'^{(i)}(\beta) = u_\theta'^{(o)}(\beta) \end{cases} \quad \text{or} \quad \begin{cases} \beta \left[ \frac{C_1}{\varepsilon} \ln(\beta) + C_2 \right] = \frac{1}{\beta} \\ \frac{C_1}{\varepsilon} [1 + \ln(\beta)] + C_2 = -\frac{1}{\beta^2} \end{cases} \quad (17)$$

whence

$$C_1 = -\frac{2\varepsilon}{\beta}; \quad C_2 = \frac{1 + 2 \ln \beta}{\beta^2} \quad (18)$$

The inner solution that we collect for the swirl velocity is therefore

$$u_\theta^{(i)} = \beta^{-2} r \left[ 1 - \ln(\beta^{-2} r^2) \right] \quad (19)$$

Assuming that the velocity at the wall is equal to the injection velocity at entry,  $u_\theta^{(o)}(1) = 1$ , a piecewise Rankine-type formulation may be arrived at by setting

$$u_\theta = \begin{cases} \frac{r}{\beta^2} \left[ 1 - \ln \left( \frac{r^2}{\beta^2} \right) \right]; & r \leq \beta \\ \frac{1}{r}; & r > \beta \end{cases} \quad \text{or} \quad u_\theta = \begin{cases} 2r \left[ 1 - \ln(2r^2) \right]; & r \leq 0.707 \\ \frac{1}{r}; & r > 0.707 \end{cases} \quad (20)$$

At first glance, Eq. (20) may be viewed as being conspicuous by its omission of viscosity. To justify its character, one may bring into perspective the Reynolds number similarity and assume that the gross characteristics of the flowfield may be taken to be independent of the viscosity at sufficiently high Reynolds numbers. Nonetheless, this hypothesis is supposed to hold far from solid boundaries, namely, in a wall-free shear flow where motion is unaffected by fluid friction. As well put by Kundu and Cohen:<sup>23</sup> “This is not true of a turbulent flow bounded by a solid wall.” Being fundamentally incomplete, Eq. (20) will be referred to as the inviscid, constant shear model (ICSM).

Equation (20) suppresses the unbounded behavior of the swirl velocity at the centerline, but it captures neither the observed increases in swirl velocity maxima nor the radial shifts in their loci.<sup>7</sup> No matter what the flow

circumstance may be, it predicts a maximum velocity of  $(u_\theta)_{\max} = 2\sqrt{2/e} \approx 1.71553$  at a constant radius of  $r_{\max} = 1/\sqrt{2e} \approx 0.428882$ . In many experiments and numerical simulations, the peak velocity can be more than double the injection speed.<sup>16-19</sup> The location of the peak is also sensitive to the inlet conditions. A more precise modulation is certainly needed and one may be established by realizing that the surface of the mantle does not necessarily delimit the free vortex region. In reality, the free vortex can be either narrower or wider, extending to an area much closer to the center of the flowfield.<sup>17,19</sup> One straightforward solution to this problem is to follow Rankine<sup>1</sup> and define a variable patch-point radius that scales with the vortex Reynolds number. As such, viscous effects can be accounted for to the extent that, given a set of experimental data, a piecewise Rankine-like solution may be readily obtained that closely resembles the observed flowfield. For the moment, we simply solve for an unspecified patch-point  $X = f(V)$ , where  $X$  is the unspecified location written as a function of the vortex Reynolds number. At the outset, Eq. (20) may be expressed as

$$u_\theta = \begin{cases} \frac{r}{X^2} \left[ 1 - \ln \left( \frac{r^2}{X^2} \right) \right]; & r \leq X \\ \frac{1}{r}; & r > X \end{cases} \quad (21)$$

In what follows, this combined vortex model will be referred to as the constant shear model (CSM). The incontrovertible analogy with Rankine's laminar model (RLM) is evident. Using our nomenclature, Rankine's combined vortex may be represented by

$$u_\theta = \begin{cases} \frac{r}{X^2}; & r \leq X \\ \frac{1}{r}; & r > X \end{cases} \quad (22)$$

Here  $X = U/\bar{u}_\theta(aX)$  is the point where the inner vortex line intersects with the sloping tail of the outer vortex. This location also defines Rankine's maximum swirl velocity  $(\bar{u}_\theta)_{\max} = \bar{u}_\theta(aX)$ . In contrast to the CSM solution which predicts constant shear throughout the core region, Rankine's model predicts constant vorticity for  $r \leq X$ .

### C. Pressure Distribution

Given that the inner core velocity is bounded at the centerline, a companion pressure may be obtained that does not exhibit the inviscid singularity of its predecessor.<sup>6</sup> From Eqs. (4) and (6), the axially and radially integrated pressures become

$$p - p(1,0) = -\int_1^r \left( u_r \frac{\partial u_r}{\partial r} + u_z \frac{\partial u_r}{\partial z} - \frac{u_\theta^2}{r} \right) dr \quad \text{and} \quad p - p(1,0) = -\int_0^z \left( u_r \frac{\partial u_z}{\partial r} + u_z \frac{\partial u_z}{\partial z} \right) dz \quad (23)$$

Integration and combination of these equations provides the pressure distribution

$$\Delta p = \begin{cases} \frac{1}{2\kappa^4 r^2} \left( r^4 \left\{ 5 + \ln \left( \frac{r^4}{X^4} \right) \left[ \ln \left( \frac{r}{X} \right) - 2 \right] \right\} - \kappa^2 X^4 \sin^2(\pi r^2) \right) - \kappa^2 \left[ 4\pi^2 z + \frac{\sin^2(\pi r^2)}{2r^2} \right] + K_1; & r \leq X \\ -\frac{1}{2r^2} \left[ 1 + \kappa^2 \sin^2(\pi r^2) \right] - \kappa^2 \left[ 4\pi^2 z + \frac{\sin^2(\pi r^2)}{2r^2} \right] + K_2; & r > X \end{cases} \quad (24)$$

where  $\Delta p = p - p(1,0)$ . The constant  $K_1$  is determined by securing the boundary condition at the origin, while  $K_2$  is calculated by setting the piecewise parts equal at  $r = X$ :

$$\begin{cases} p(1,0) = -\frac{1}{2} + K_2 = 0 \\ p(X,0) = K_1 + 3X^{-2} = K_2 \end{cases} \quad \text{or} \quad \begin{cases} K_1 = \frac{1}{2} - 3X^{-2} \\ K_2 = \frac{1}{2} \end{cases} \quad (25)$$

We hence extract the piecewise distribution

$$\Delta p = \begin{cases} \frac{1}{2} - \frac{3}{X^2} + \frac{1}{2\kappa^4 r^2} \left( r^4 \left\{ 5 + \ln \left( \frac{r^4}{X^4} \right) \left[ \ln \left( \frac{r}{X} \right) - 2 \right] \right\} - \kappa^2 X^4 \sin^2(\pi r^2) \right) - \kappa^2 \left[ 4\pi^2 z + \frac{\sin^2(\pi r^2)}{2r^2} \right]; & r \leq X \\ \frac{1}{2} - \frac{1}{2r^2} \left[ 1 + \kappa^2 \sin^2(\pi r^2) \right] - \kappa^2 \left[ 4\pi^2 z + \frac{\sin^2(\pi r^2)}{2r^2} \right]; & r > X \end{cases} \quad (26)$$

## IV. Results and Discussion

### A. Laminar Core Model (LCM) Representation

To illustrate the ability of the heuristic solution to embody different models, we start by reproducing the laminar core boundary layer model derived by Vyas, Majdalani and Chiaverini.<sup>8</sup> Clearly, if we are to claim a portable solution, the swirl velocity calculated from the present work must approximate key features connected with the boundary layer model. For a simple demonstration of the matching paradigm, we implement the notion that swirl velocities from the laminar and constant shear models must exhibit the same maxima. This is achieved by first setting the derivatives of both models equal to zero and solving for the corresponding radii. While the inner part of the piecewise velocity yields

$$\left. \frac{du_\theta}{dr} \right|_{r=r_{\max}} = 0 \quad \text{or} \quad r_{\max} = \frac{X}{\sqrt{e}} \quad (27)$$

the laminar model projects

$$r_{\max} = \sqrt{\frac{2}{V} \left[ -1 - 2 \operatorname{pln} \left( -1, -\frac{1}{2} e^{-\frac{1}{2}} \right) \right]} \approx \frac{2.24181}{\sqrt{V}} \quad (28)$$

These positions can be substituted back into their respective equations and then set equal to each other. One gets

$$\frac{2}{Xe^{\frac{1}{2}}} = 1 - e^{\frac{1}{2} + \operatorname{pln} \left( -1, -\frac{1}{2} e^{-\frac{1}{2}} \right)} \sqrt{\frac{-V}{2 \left[ 1 + 2 \operatorname{pln} \left( -1, -\frac{1}{2} e^{-\frac{1}{2}} \right) \right]}} \quad (29)$$

Equation (29) enables us to solve for  $X$  as a function of  $V$  directly from

$$X = \frac{2}{\sqrt{eV}} \frac{\sqrt{-2 \left[ 1 + 2 \operatorname{pln} \left( -1, -\frac{1}{2} e^{-\frac{1}{2}} \right) \right]}}{\left\{ 1 - \exp \left[ \frac{1}{2} + \operatorname{pln} \left( -1, -\frac{1}{2} e^{-\frac{1}{2}} \right) \right] \right\}} \approx \frac{3.80167}{\sqrt{V}} \quad (30)$$

This Rankine-like patch-point  $X$  permits our piecewise velocity to capture the same peak velocity that the laminar boundary layer solution projects as a function of  $V$ .

A comparison of the different swirl velocity models at four increasing vortex Reynolds numbers is presented in Fig. 2. While the free vortex is invariant with respect to  $V$ , both the present study (CSM) and the laminar boundary

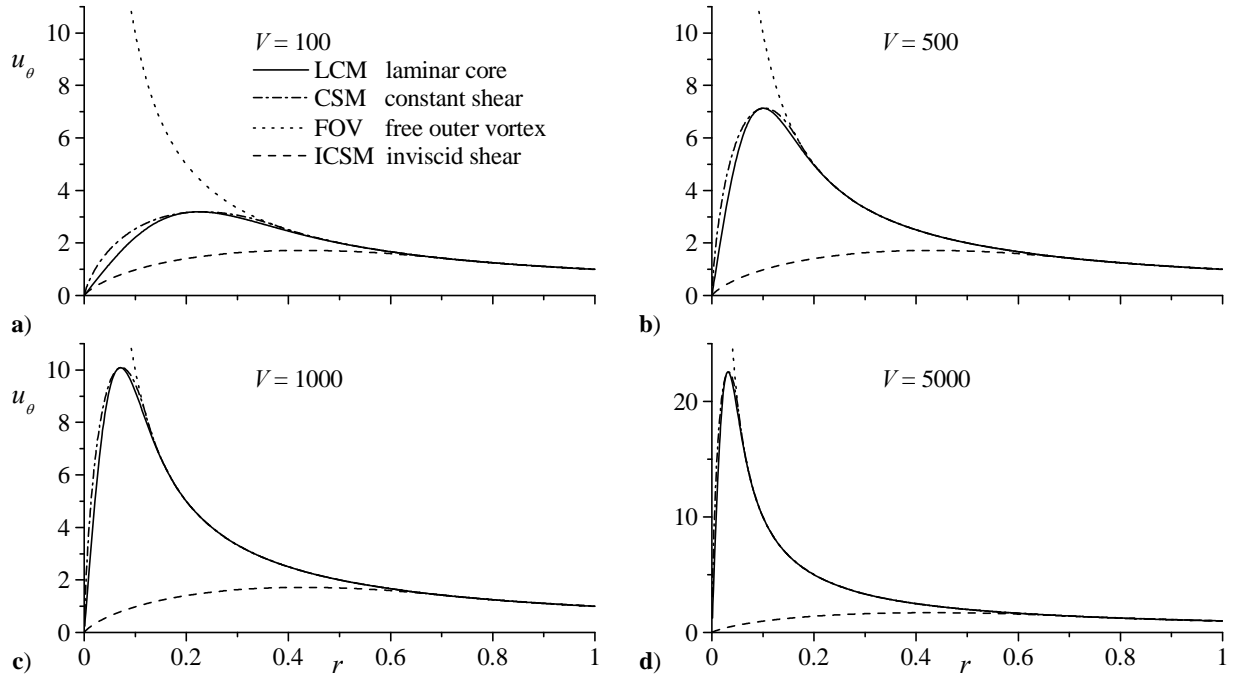


**Figure 2. Velocity comparison at several vortex Reynolds numbers illustrating the ability to duplicate laminar behavior.**

layer model (LCM) capture the increasing velocity peaks and their translation toward the centerline with successive increases in  $V$ . Note that the two models match identically at the point of highest velocity, owing to the imposed patch-point treatment. They also behave rather similarly elsewhere in the domain. The incomplete ICSM model remains invariant throughout, thus establishing a low-end datum for the velocities. This ICSM baseline is difficult to undershoot without exiting the range of meaningful vortex Reynolds numbers (below  $V \approx 90$ ).

Figure 3 compares the pressure distributions of the two models at two vortex Reynolds numbers. It also displays the ICSM prediction. The radial pressure gradient in Fig. 3a is slightly higher in the case of the constant shear model, especially in the core region. This behavior can be accounted for by the slightly increased velocity anticipated from the piecewise model near the centerline. The noted increase is magnified by squaring the velocity and dividing by the small distances near the core, as per the last term on the right-hand-side of Eq. (23). Except for these differences, the piecewise model faithfully captures the general shape of the radial pressure distribution. The actual pressure drop is shown in Fig. 3b. The CSM pressure starts slightly higher, but then quickly diminishes to match the LCM approximation. The ICMS model remains flat, displaying a weaker sensitivity to spatial variations and an indifference to the Reynolds number. It should be noted that the CSM solution offers one degree of freedom that can be adjusted to suit a particular application. For example, should accurate prediction of the pressure stand as the most valuable requirement for a specific problem, then the patch-point radius could be adjusted to best fit the experimental pressure data near the core. A similar patching paradigm is used in modeling large atmospheric flows where only pressure related measurements are available.

Before concluding this comparison, it may be instructive to examine the behavior of shear and vorticity near the axis of rotation. In view of the shear stress being a quintessential contributor in the derivation of the CSM approximation, we compare the present result to the LCM solution by Vyas, Majdalani and Chiaverini.<sup>8</sup> The latter is given by

$$\tau_{r\theta} = -2\varepsilon r^{-2} \left[ 1 - \left( 1 + \frac{1}{4} r^2 V \right) e^{-\frac{1}{4} V r^2} \right] \quad (31)$$

Since only amendments to the swirl velocity are considered here, the affected member of the shear stress tensor is  $\tau_{r\theta}$ . Recalling the general form from Eq. (14), we find after substitution

$$\tau_{r\theta} = \varepsilon r \frac{\partial}{\partial r} \left( \frac{u_\theta}{r} \right) = \begin{cases} -\frac{2\varepsilon}{X^2}; & r \leq X \\ -\frac{2\varepsilon}{r^2}; & r > X \end{cases} \quad (32)$$

For the vorticity, we similarly find

$$\Omega_z = \frac{1}{r} \frac{\partial(r u_\theta)}{\partial r} = \begin{cases} -\frac{4}{X^2} \ln\left(\frac{r}{X}\right); & r \leq X \\ 0; & r > X \end{cases} \quad (33)$$

The resultant curves are plotted in Fig. 4 and compared to the results of the LCM treatment, namely, to  $\Omega_z = \frac{1}{2} V \exp\left(-\frac{1}{4} V r^2\right)$ . In both parts of Fig. 4, we see that past the patch-point radius, a good agreement between the models is realized. Closer to the core, a deviation is manifested as a result of the constant shear stress model becoming uniform. As shown in Fig. 4a, the constant core value of the absolute shear  $|\tau_{r\theta}|$  is slightly lower than the maximum LCM value. Aside from this disparity near the centerline, the CSM and LCM curves are concurrent

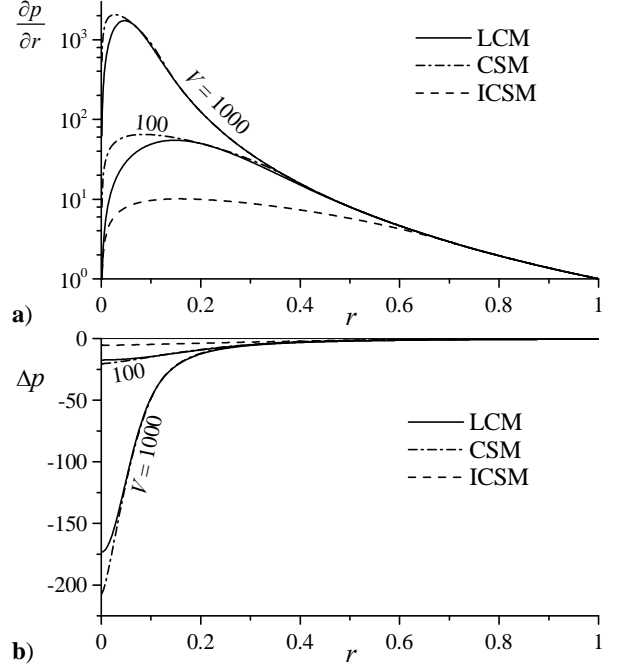


**Figure 3. Model comparison for a) the radial pressure gradient and b) the pressure distribution.**

elsewhere in the domain. Here too, the ICSM shear is seen to be the smallest. In Fig. 4b, the vorticity prescribed by the piecewise model is seen to mimic the LCM curve. However, unlike the laminar model which smoothly tapers off in the vicinity of the core, the CSM vorticity does not approach a constant as  $r \rightarrow 0$ . This inability to predict solid body rotation near the axis of the chamber may be regarded as a weakness in the CSM representation.

### B. Heuristic Turbulent Model Representation

One of the chief attributes of the piecewise solution stems from its display of a single degree of freedom that can be tuned for better performance. For example, knowing that the laminar boundary layer treatment can overpredict the velocity distribution near the core when the flow is turbulent, a heuristic correction can be sought. One avenue to resolve this issue when  $V$  is large is to introduce an effective turbulent vortex Reynolds number that will be larger than its laminar counterpart. The actual turbulent Reynolds number based on laboratory tests could thus be converted into a smaller effective value that would be suitably retrofitted into the laminar model. The development of such an approximation must of course be based on reliable experimental measurements and numerical simulations. Alternatively, one may assume that the laminar model accurately predicts the thickness of the forced vortex,  $\delta_c = r_{\max}$ , given by Eq. (28). Then, considering that the constant shear region must scale with  $\delta_c$ , one may let  $X = \lambda \delta_c$ , where  $\lambda$  is taken to match actual observations. To illustrate this point, the velocities in Fig. 5 are compared using  $\lambda = 3$ ; such a value implies that the core region over which the shear stress remains uniform is thrice the thickness of the forced vortex. This

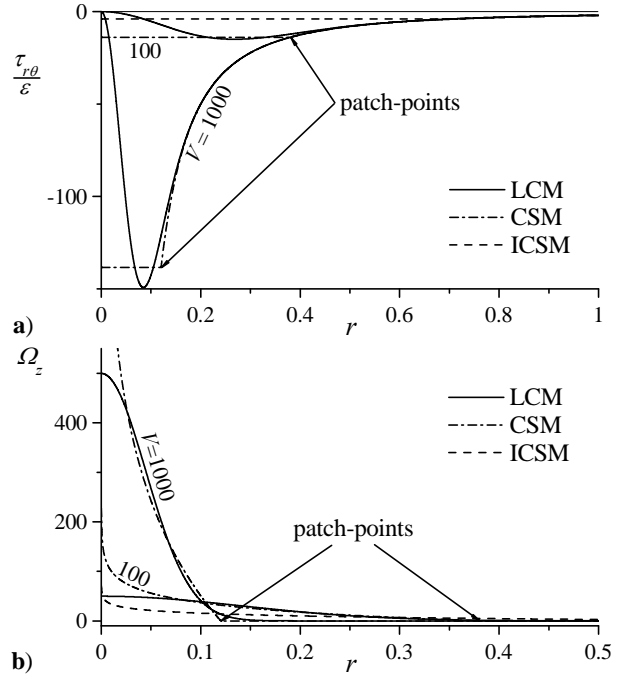


**Figure 4. Model comparison for a) the shear stress and b) the axial component of vorticity.**

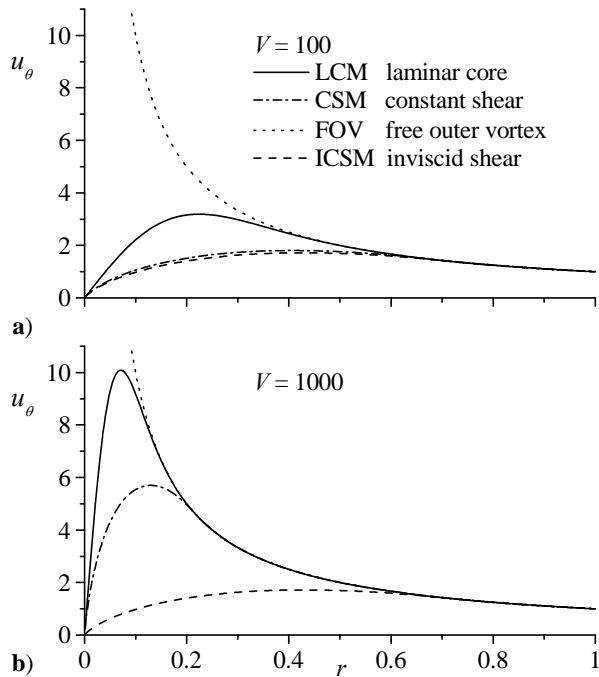


**Figure 5. Velocity comparison at two Reynolds numbers illustrating turbulent ( $\lambda = 3$ ) vs. laminar behavior.**

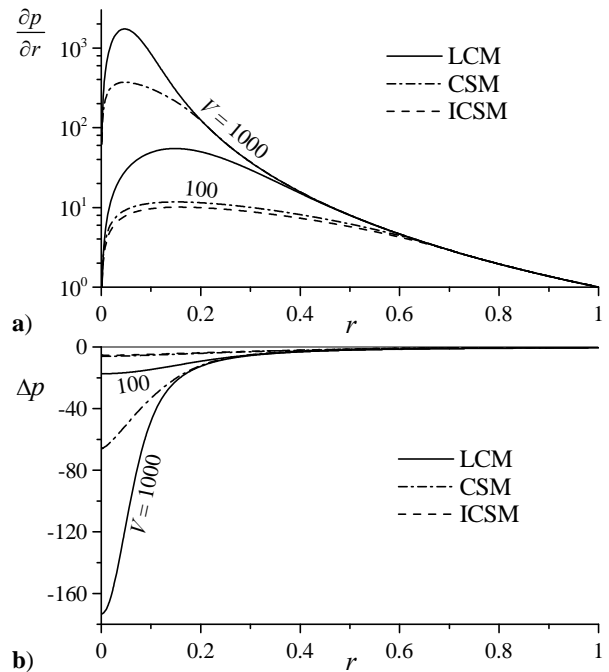


**Figure 6. Pressure comparison at two Reynolds numbers illustrating turbulent ( $\lambda = 3$ ) vs. laminar behavior.**

notion enables us to fit the empirical data without specifically solving a complicated turbulent model. As seen in Fig. 5, the heuristic CSM model will, under these conditions, predict lower maximum velocities than projected by laminar theory. In Fig. 5a, the CSM curve almost directly coincides with the fixed ICSM solution, given a low vortex Reynolds number of 100. When the latter is increased by one order of magnitude in Fig. 5b, the peak CSM velocity is seen to increase, but not as rapidly as the laminar solution. The same may be said of the radial pressure gradient and its distribution shown in Fig. 6. For the low vortex Reynolds number case, it is interesting that the heuristic CSM model can match rather well the ICSM line. In fact, one may solve for the value of  $V$  that reproduces the ICSM value by evaluating Eq. (28) at the mantle. One finds

$$X = \frac{2.24181\lambda}{\sqrt{V}} \quad (34)$$

Thus using  $\lambda = 3$  and  $X = 1/\sqrt{2}$ , one retrieves the rather low Reynolds number of  $V = 90.463$ . Later, when  $V$  is increased by one order of magnitude, a departure is noted wherein the heuristic CSM model is seen to occupy an intermediate position between the laminar and purely inviscid solutions. The shear stress and vorticity associated with the heuristic model are also found to be conservative by comparison with the LCM projections. These are illustrated in Figs. 7a and 7b.

It should be duly noted that the heuristic approach presented here is not yet tested, and other reconciliatory schemes may be arrived at. The CSM swirl velocity overshoot and location must be thoroughly interrogated for validity via comparisons to experimental and robust computational predictions. Another model that may be pursued consists of calculating the patch-point radius such that the integrated shear stress associated with the CSM approximation can be made to match the corresponding value predicted by the LCM solution. At the outset, the surface areas under the  $\tau_{r\theta}$  curves in Fig. 4a will be matched. Whether such a scheme could produce a more accurate approximation will remain a matter of conjecture until such time when the model is compared to a sufficiently large collection of experimental and numerical data. In like fashion, the pressure distribution could also be used as the target function for the model. As alluded to earlier, one may attempt to match pressure profiles such as those arising in Fig. 6 to the observed patterns. In short, the patch-point radius could be adjusted in a variety of ways to best fit laboratory or numerical experiments.

Before leaving this subject, it may be useful to note that with the onset of turbulence, the models presented heretofore become practical approximations at best. When the core flow is turbularized, it will be difficult to state

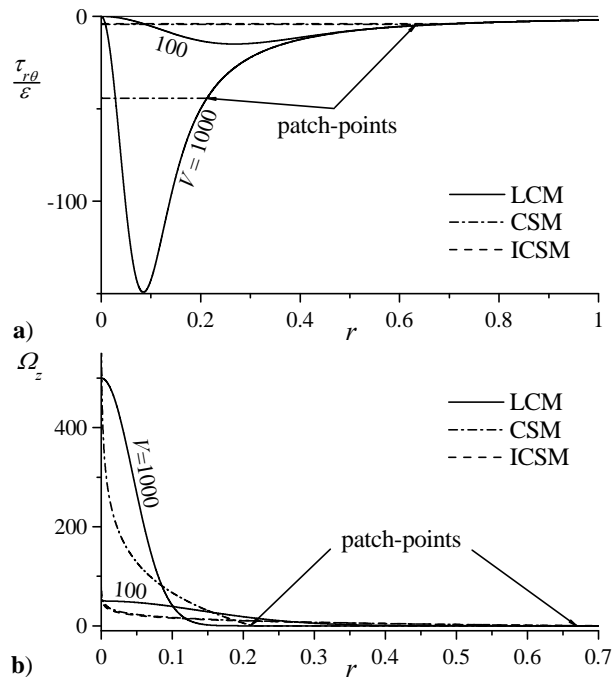


**Figure 7. Comparison for a) the shear stress and b) the axial component of vorticity at two Reynolds numbers illustrating turbulent ( $\lambda = 3$ ) vs. laminar behavior.**

with certainty that the outer, annular flow remains irrotational, even if partly so. A turbulent flow has the ability to attract the surrounding irrotational fluid inwardly through frictional effects, specifically through a process known as entrainment. While the source of entrainment may be ascribed to viscous shear in laminar flows, it is mostly inertial in turbulent flows. In fact, the entrainment rate under turbulent conditions can far exceed any effects that are attributable to fluid friction. After the irrotational outer fluid is drawn into the turbulent core, the new fluid is turbularized by the introduction of small viscous eddies that form at the interface between the rotational and irrotational regions. In the bidirectional vortex chamber, the turbulent core can therefore entrain the irrotational annular flow to the extent of causing further departures from the established solutions.

### C. Analogy with the Rankine Model

Figure 8 compares the shapes of the swirl velocity profiles for the LCM and CSM solutions to Rankine's. In order to draw meaningful comparisons, both dependent and independent variables are renormalized. First, the radial coordinate is normalized by  $r_{\max}$  such that the maximum velocity occurs at a value of unity. Second, each velocity is divided by its respective peak value in

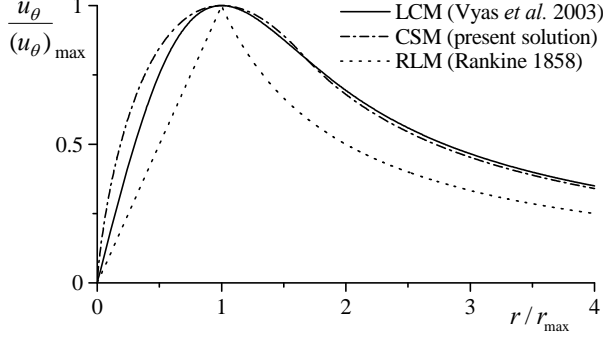


**Figure 8. Optimally rescaled swirl velocity profiles for the laminar core model (LCM), constant shear model (CSM), and Rankine laminar model (RLM).**

Instead, the tangential velocity at the sidewall remains equal to the circumferential injection speed,  $\bar{u}_\theta(a, \bar{z}) = U$ . This particular requirement coincides with the wall boundary condition that one would impose in a centrifuge where the cyclonic motion is induced by the rotating sidewall. The corresponding circular speed may be calculated to be  $\varpi = U/a$ . A model that more adequately captures the behavior of the bulk gas motion in the VCCWC engine is one that assumes a stationary sidewall. The wall-bounded counterpart of the present solution may hence be obtained by combining the CSM-based core approximation with an outer, annular profile that observes the velocity adherence condition. Such profile may be directly obtained from the work of Vyas and Majdalani<sup>7</sup> for the tangential velocity. Furthermore, the axial and radial velocity components may be asymptotically enhanced to account for the confining wall. As shown in the companion paper by Batterson and Majdalani,<sup>10</sup> a wall-bounded solution may be arrived at using the tools of matched-asymptotic expansions. At length, a uniformly valid wall-to-wall approximation may be constructed in which the three components of the velocity are given by

$$\begin{cases} u_r = -\frac{\kappa}{r} \sin(\pi r^2) \left[ 1 - e^{-\frac{1}{2}(\frac{1}{6}\pi^2 - 1)V(1-r^2)} \right] & u_z = 2\pi\kappa z \cos(\pi r^2) \left[ 1 - e^{-\frac{1}{4}(\frac{1}{6}\pi^2 - 1)V(1-r^2)} \right] \\ u_\theta = \begin{cases} \frac{r}{X^2} \left[ 1 - 2 \ln\left(\frac{r}{X}\right) \right]; & r \leq X \\ \frac{1}{r} \left[ 1 - e^{-\frac{1}{4}(\frac{1}{6}\pi^2 - 1)V(1-r^2)} \right]; & r > X \end{cases} \end{cases} \quad (35)$$

Equation (35) is a modified form of the CSM approximation that is rectified so as to satisfy the no slip condition. It will closely resemble Eqs. (21) and (10) except in the vicinity of the sidewall.

## V. Conclusions

In this article, a heuristic formulation for the swirl velocity of the bidirectional vortex is presented and discussed. A constant shear stress model is employed to extract the velocity near the core, which is then patched to an outer solution that is mainly irrotational. The ensuing approximation exhibits one degree of freedom that grants us the possibility to anchor our solution for a given flow pattern. This predictive feature is set by relating the patch-point radius of the constant shear model to the vortex Reynolds number arising in a given application. Since the patch-point radius delimits the inner zone where the shear stress may be taken to be uniform, linking this radius to the vortex Reynolds number enables us to control the thickness of the core region along with the maximum speed that the tangential velocity can reach. The unspecified patch-point radius imparts our heuristic model with the ability to conform to a nearly arbitrary swirl pattern over a practical range of Reynolds numbers.

While the present solution offers a useful compromise between the simplicity of the laminar core layer model and the validity of the constant shear stress model at high Reynolds numbers, it also has some drawbacks. The most obvious of these is the piecewise character of the swirl velocity. Further extensions to the solution, such as compressible corrections, will also have to be piecewise in nature. Another shortcoming stands in its inability to predict solid body rotation near the core. To improve this model, more work lies ahead, particularly in the need to canvas the literature for turbulent flow data and to set up experiments that can validate and help to refine the present analysis.

order to enforce uniformity of height. The unified normalization used here enables us to capture the basic similarities shared by these profiles. While the combined Rankine model consists of patching the forced vortex line with the outer vortex, both LCM and CSM curves represent smooth blending of the inner and outer regions. In conformance with turbulent flow theory, a slight bulging or flattening of the CSM velocity is observed (chained line) in relation to the laminar models (solid or broken lines).

## D. Wall-to-Wall, Uniformly Valid Representation

The swirl velocity described above appears to be a viable model for the bidirectional vortex core. However, it does not satisfy the no-slip condition at the wall.

## Acknowledgments

We are deeply grateful for the support received from ORBITEC (FA8650-05-C-2612) and the National Science Foundation (CMS-0353518). We are especially thankful for valuable discussions with Martin J. Chiaverini, Principal Propulsion Engineer, and William H. Knuth, Chief Engineer, Orbital Technologies Corporation, Madison, Wisconsin. We also wish to acknowledge much valued assistance received from Erin K. Halpenny in preparing the final version of the manuscript.

## References

- <sup>1</sup>Rankine, W. J. M., *A Manual of Applied Mechanics*, 9th ed., C. Griffin and Co., London, UK, 1858.
- <sup>2</sup>Penner, S. S., "Elementary Considerations of the Fluid Mechanics of Tornadoes and Hurricanes," *Acta Astronautica*, Vol. 17, 1972, pp. 351-362.
- <sup>3</sup>Königl, A., "Stellar and Galactic Jets: Theoretical Issues," *Canadian Journal of Physics*, Vol. 64, 1986, pp. 362-368.
- <sup>4</sup>ter Linden, A. J., "Investigations into Cyclone Dust Collectors," *Proceedings of the Institution of Mechanical Engineers*, Vol. 160, 1949, pp. 233-251.
- <sup>5</sup>Bloor, M. I. G., and Ingham, D. B., "The Flow in Industrial Cyclones," *Journal of Fluid Mechanics*, Vol. 178, No. 1, 1987, pp. 507-519.
- <sup>6</sup>Vyas, A. B., and Majdalani, J., "Exact Solution of the Bidirectional Vortex," *AIAA Journal*, Vol. 44, No. 10, 2006, pp. 2208-2216.
- <sup>7</sup>Vyas, A. B., and Majdalani, J., "Characterization of the Tangential Boundary Layers in the Bidirectional Vortex Thrust Chamber," AIAA Paper 2006-4888, July 2006.
- <sup>8</sup>Vyas, A. B., Majdalani, J., and Chiaverini, M. J., "The Bidirectional Vortex. Part 2: Viscous Core Corrections," AIAA Paper 2003-5053, July 2003.
- <sup>9</sup>Majdalani, J., and Rienstra, S. W., "On the Bidirectional Vortex and Other Similarity Solutions in Spherical Coordinates," *Journal of Applied Mathematics and Physics (ZAMP)*, Vol. 58, No. 2, 2007, pp. 289-308.
- <sup>10</sup>Batterson, J. W., and Majdalani, J., "On the Boundary Layers of the Bidirectional Vortex " AIAA Paper 2007-4123 June 2007.
- <sup>11</sup>Chiaverini, M. J., Malecki, M. J., Sauer, J. A., Knuth, W. H., and Majdalani, J., "Vortex Thrust Chamber Testing and Analysis for O<sub>2</sub>-H<sub>2</sub> Propulsion Applications," AIAA Paper 2003-4473, July 2003.
- <sup>12</sup>Vatistas, G. H., Lin, S., and Kwok, C. K., "Theoretical and Experimental Studies on Vortex Chamber Flows," *AIAA Journal*, Vol. 24, No. 4, 1986, pp. 635-642.
- <sup>13</sup>Ogawa, A., "Estimation of the Collection Efficiencies of the Three Types of the Cyclone Dust Collectors from the Standpoint of the Flow Pattern in the Cylindrical Cyclone Dust Collectors," *Bulletin of the JSME*, Vol. 27, No. 223, 1984, pp. 64-69.
- <sup>14</sup>Hoekstra, A. J., Van Vliet, E., Derksen, J. J., and Van den Akker, H. E. A., "Vortex Core Precession in a Gas Cyclone," *Advances in Turbulence, VII*, edited by U. Frisch, Kluwer, Dordrecht, The Netherlands, 1998, pp. 289-292.
- <sup>15</sup>Derksen, J. J., and Van den Akker, H. E. A., "Simulation of Vortex Core Precession in a Reverse Flow Cyclone," *American Institute of Chemical Engineers*, Vol. 46, No. 7, 2000, pp. 1317-1331.
- <sup>16</sup>Fang, D., Majdalani, J., and Chiaverini, M. J., "Simulation of the Cold-Wall Swirl Driven Combustion Chamber," AIAA Paper 2003-5055, July 2003.
- <sup>17</sup>Rom, C. J., Anderson, M. H., and Chiaverini, M. J., "Cold Flow Analysis of a Vortex Chamber Engine for Gelled Propellant Combustor Applications," AIAA Paper 2004-3359, July 2004.
- <sup>18</sup>Murray, A. L., Gudgen, A. J., Chiaverini, M. J., Sauer, J. A., and Knuth, W. H., "Numerical Code Development for Simulating Gel Propellant Combustion Processes," JANNAP, May 2004.
- <sup>19</sup>Hu, L. Y., Zhou, L. X., Zhang, J., and Shi, M. X., "Studies of Strongly Swirling Flows in the Full Space of a Volute Cyclone Separator," *AIChE Journal*, Vol. 51, No. 3, 2005, pp. 740-749.
- <sup>20</sup>Townsend, A. A., *The Structure of Turbulent Shear Flow*, Cambridge University Press, Cambridge, UK, 1976.
- <sup>21</sup>Tennekes, H., and Lumley, J. L., *A First Course in Turbulence*, MIT Press, Cambridge, MA, 1976.
- <sup>22</sup>White, F. M., *Viscous Fluid Flow*, McGraw-Hill, New York, 1991.
- <sup>23</sup>Kundu, P. K., and Cohen, I. M., *Fluid Mechanics*, 2nd ed., Academic Press, San Diego, California, 2002.